Line-shape parameters and their temperature dependence for self-broadened CO2 lines in the 296 K-1250 K range by requantized classical molecular dynamics simulations

N.H. Ngo, H. Tran

Line-shape parameters and their temperature dependence for self-broadened CO_2 lines in the 300 K - 1250 K range by requantized classical molecular dynamics simulations

N.H. Ngo[1,2], H. Tran[3]

[1] *Faculty of Physics, Hanoi National University of Education, 136 Xuan Thuy Street, Cau Giay District, Hanoi, Vietnam*

[2] *Institute of Natural Sciences, Hanoi National University of Education, 136 Xuan Thuy Street, Cau Giay, Hanoi, Vietnam*

[3] *Laboratoire de Météorologie Dynamique/IPSL, CNRS, Sorbonne Universités, École normale supérieure, PSL Research University, École polytechnique, F-75005 Paris, France*

Corresponding author: hoa.nn@hnue.edu.vn, ha.tran@lmd.jussieu.fr

Abstract

Line-shape parameters for self-broadened CO_2 transitions are predicted for temperatures ranging from 296 K to 1250 K, using requantized molecular dynamics simulations (rCMDS). The line broadening coefficient, the speed dependence component and the first-order line-mixing coefficient for lines with rotational quantum number from 2 to 100, have been determined from fits of the rCMDS spectra with the Voigt and speed dependent Voigt profiles. These parameters and their temperature dependences were compared with recent high-quality measurements at both room and high temperatures, showing good agreements for all considered parameters. In particular, this study highlights that the temperature dependence of the speed dependent Voigt line broadening coefficient in the HITRAN database needs to be corrected. Additionally, we demonstrate that the temperature dependence for the speed dependence of the line broadening differs from that of the line broadening, contrary to the assumption widely used in the literature. These findings confirm the quality of theoretical predictions using rCMDS. The data provided can be used to complete and improve spectroscopic databases for various applications.

1. Introduction

Precise modeling of infrared absorption by carbon dioxide at high temperature is crucial for radiative transfer calculations for the atmosphere of Venus [1] and for studying combustion media where CO_2 is a significant component [2]. For these applications, accurate line-shape parameters of self-broadened CO_2 and their temperature dependences are essential.

Self-broadening parameters for infrared CO_2 lines have been investigated in numerous experimental studies (e.g. [3-14]), but most of these studies have focused on room temperature or earth atmospheric temperature conditions. To the best of our knowledge, high-temperature line-shape parameters for pure CO_2 have been measured in [4,15,16]. The self-broadening coefficient of the $R(50)$ line of the $\nu_1 + 2\nu_2 + \nu_3$ band was measured at 1500 K in Ref. [15]. In [4] the $R(28)$ and $P(70)$ lines of the $\nu_1 + \nu_3$ band were measured at temperatures up to 1200 K. In Ref. [16], spectra of pure CO_2 in the 6800-7000 cm^{-1} region were measured at temperatures up to 980 K. Line-shape parameters were obtained for more than 40 lines of the $3\nu_3$ band and 75 lines of the $\nu_2 + 3\nu_3 - \nu_2$ hot band by fitting the measured spectra with the Voigt (V) and speed dependent Voigt (sdV) profiles. The temperature dependences of the line broadening and shifting were also derived, using a single power law. This study represents the most complete experimental investigation of line-shape

parameters for pure CO_2 at high temperature and moderate densities (corresponding to pressures below 1 atm, where lines are relatively isolated). CO_2 self-broadening coefficients were calculated in Ref. [17] using a semi-classical method. These calculations covered several bands, for lines with J up to 160 and for a wide temperature range, from 200 K to 2000 K. The parameters correspond to those of the Voigt profile. Comparisons between these theoretical results and the experimental values from Ref. [16] show good agreements for the line broadening coefficients at room temperature while rather significant differences are observed for the temperature dependence of the line broadening [16].

In the HITRAN database [18], CO_2 line-shape parameters and their temperature dependence associated with the Voigt and the sdV profiles are provided. These parameters are derived by fitting a Padé approximant to measured or calculated data available in the literature. For the Voigt profile, the room temperature broadening coefficients are based on a Padé approximant of the measured data from Ref. [19] and extrapolated for non-measured lines with $J > 60$ [20]. The temperature dependence is modeled as a Padé approximant of the semi-classically calculated values from Ref. [8], which have been shown to agree well with values derived from spectra measured in the 258 K - 296 K range [8]. For the sdV profile, room temperature broadening coefficients and their speed dependent components are obtained from measured data of Ref. [14] and extrapolated for high J lines. Note that in the HITRAN database, the vibrational dependence of CO_2 line broadening coefficients is generally neglected, except for the $3\nu_3$ band, which was treated separately [18]. The temperature dependence of the sdV line broadening coefficient in HITRAN is derived from measured data of Ref. [12], which were deduced from spectra recorded in the 170 K - 296 K range. Consequently, several extrapolations are necessary to estimate line broadening coefficients at high temperature and/or for high J lines.

Recent works conducted by our group have demonstrated that classical molecular dynamics simulations (CMDS), when combined with a requantization procedure, can accurately predict line-shape parameters and their temperature dependences for linear molecular systems such as CO_2, N_2O and CO [21-24]. It has been shown that these CMDS can predict not only line broadening coefficients but also more refined line-shape parameters, including the speed dependence of the line width, Dicke narrowing and line-mixing coefficients. For example, predictions for N_2-broadened CO_2 lines are in very good agreement with values obtained from high quality measurements [21]. These CMDS, based on an intermolecular potential, Newtonian equations of motion and a requantization procedure, enable the calculation of the spectral density under specific pressure and temperature conditions. The resulting spectra can then be fitted with a line-shape model to retrieve the corresponding line-shape parameters. In this work, these simulations will be applied for the first time to predict line-shape parameters for self-broadened CO_2 at high temperature, up to 1250 K. These predictions will be compared with recent experimental results from Ref. [16] and with values of the HITRAN database [18].

This paper is organized as follows: Section 2 presents the calculation method, including a description of the analysis procedure for the predicted spectra. Section 3 discusses the obtained line-shape parameters and their comparisons with existing data. Finally, section 4 provides the conclusions and future perspectives of this work.

2. Calculations and analysis

2.1 Requantized classical molecular dynamics simulations for pure CO_2

Classical molecular dynamics simulations were performed for pure CO_2 at 1 atm and for various temperatures: 296 K, 500 K, 750 K, 1000 K and 1250 K. We used the same calculation principle and procedure as what were done in Refs. [25,26] in which detailed descriptions of the calculations can be found. The site-site interaction potential from Ref. [27] has been retained here to represent the intermolecular interactions. This potential was chosen because it provided the best agreement with measured data among several potentials used for collision-induced absorptions in the far-infrared band of CO_2 [28]. In Ref. [26], we demonstrated that different intermolecular potentials produced nearly identical Lorentzian broadening coefficients at room temperature. The impact of the potential as well as of its different contributions on the predicted line shapes at high temperatures is the subject of a forthcoming study and will not be discussed in this paper.

Calculations were performed using the Jean Zay HPE SGI 8600 supercomputer at the *Institut du Dévéloppement et des Ressources en Informatique Scientifique*, which supports massively parallel computing. For each temperature, a total of 240×10^6 molecules were considered, achieving a signal to noise ratio of up to 1000 for the calculated spectra. The molecules, treated as rigid rotors, were distributed across twelve thousand boxes, each containing 20 000 molecules. Initially, the molecules were randomly placed in the boxes with the constraint that they should be separated by at least 9 Å in order to prevent unphysically strong interactions. This requires a relaxation period, or a "temporization time", for the system to reach equilibrium. The value of this temporization time depends on the temperature, for instance, at 1000 K, this time is approximately 50 ps. Translational and angular speeds verifying the Maxwell-Boltzmann distribution were initialized while random center-of-mass velocity vectors and molecular axis orientation were assigned. The parameters describing the classical state of each molecule (i.e. center-of-mass position, velocity, angular momentum, and molecular axis orientation) were then computed for each time step, up to a maximum time t_{max} (e.g. at 1000 K, the used time step is about 1.5 fs while t_{max} is 1200 ps). A requantization procedure, as described in Ref. [25], was applied to the classical rotation of the molecules. In this procedure, an even and integer rotational quantum number J is determined from the classical rotational energy of a molecule. Once J is identified, the classical angular momentum ω is requantized by replacing it with $\hbar J/I$ where I is the moment of inertia, the orientation of $\vec{\omega}$ being kept unchanged. This requantization process corresponds to matching the rotational frequency with the quantum position of the P branch lines (this implies that the calculated R branch will be the exact symmetric of the P branch). We then calculated the auto-correlation function of the dipole moment, from the temporization time to t_{max}. The Doppler effect associated with the translational motion was also incorporated into the auto-correlation function, as shown in Eq. (3) of Ref. [25]. For each temperature, three values of the Doppler width Γ_D (e.g. $\Gamma_D = 5.71\ 10^{-3}$, $1.14\ 10^{-2}$ and $1.71\ 10^{-2}$ cm^{-1} at 296 K) were used in the calculations. This approach yielded three values of the ratio Γ_D/Γ_L for each line (e.g., ranging from about 0.07 to 0.22 at room temperature, Γ_L being the Lorentz width). Since all the effects of vibrational motion were disregarded in our rCMDS, this effectively corresponds to three calculations at three different pressures with a single Doppler width, thereby reducing computational time. The absorption coefficient was obtained by performing the Fourier-Laplace transform of the auto-correlation function of the dipole moment, without employing any adjustable parameters. It is important to note that the spectra calculated using rCMDS do not show any pressure shift (at least the vibrational part, which is the primary contribution of pressure shift). This is because our rCMDS do not account for dipole

dephasing, which arises from differing effects of intermolecular interactions on molecules in the upper and lower states of optical transitions.

2.2 Spectra analysis

For each temperature, the spectra calculated by rCMDS were fitted using the Voigt and speed dependent Voigt (sdV) profiles, including the first-order line-mixing parameter, through a multi-spectrum fitting procedure. For each line, the following parameters were fitted: the collisional line broadening γ_0 (cm^{-1}/atm), its speed dependent component γ_2 (cm^{-1}/atm), the first-order line-mixing coefficient ζ (atm^{-1}), the maximum line absorption position (σ_0), and line area (A). The Doppler width was fixed to its calculated value. The three spectra computed for three values of Γ_D were simultaneously fitted, with the line-shape parameters constrained to be the same for each line, while σ_0 and A were independently retrieved for each line and spectrum. All lines in the computed spectrum (i.e. the P branch spectrum, since the R branch is its exact symmetric counterpart) were fitted simultaneously. A linear base line (versus the relative wavenumber) was also adjusted for each spectrum. Tests conducted with smaller spectral ranges showed negligible impact on the retrieved line-shape parameters, which is accounted for in the reported uncertainty. Note that the speed dependent Nelkin-Ghatak profile was also used to fit the rCMDS-computed spectra but resulted in similar fit residuals as the SDV model. This is likely due to the considered Γ_D/Γ_L range and the limited signal to noise ratio of our simulated spectra.

From the line-shape parameters retrieved for each temperature, their temperature dependences were then determined using a single power law, i.e. $A(T) = A(T_0)(\frac{T_0}{T})^{n_A}$ where $T_0 = 296\,K$, $A(T)$ represents either γ_0 or γ_2, and n_A is the corresponding temperature dependence exponent. Note that tests using the double power law [29] showed no improvement in modeling the temperature dependence of these parameters. For the first-order line-mixing parameter, ζ, a simplified form of the double power law is used, as detailed in sub-section 3.4. The obtained line-shape parameters and their temperature dependences are presented and discussed in the next section.

Figures 1 and 2 display the rCMDS-calculated spectra at 500 K and 1250 K, along with the residuals obtained from their fits using the Voigt and sdV models. The results show that the sdV model leads to good fits of the rCMDS spectra, the remaining residuals are mostly due to numerical noise in the calculations.

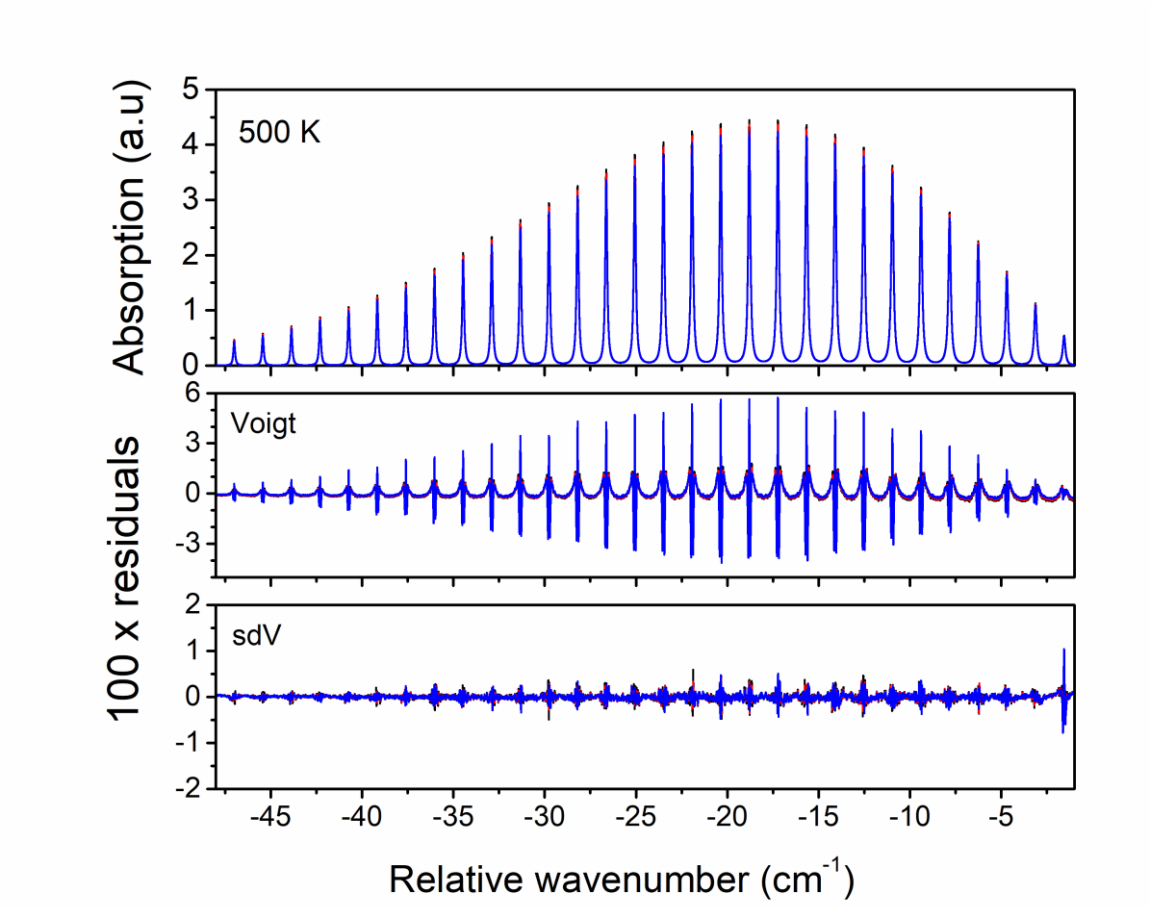

Figure 1: The top panel shows spectra of self-broadened CO_2 calculated by rCMDS at 500 K and 1 atm, for three values of the Doppler width, i.e. $\Gamma_D = 7.42\ 10^{-3}$, $1.48\ 10^{-2}$ and $2.23\ 10^{-2}$ cm^{-1}. The middle and bottom panels display the residuals obtained from fitting these spectra with the Voigt and the sdV profiles, respectively.

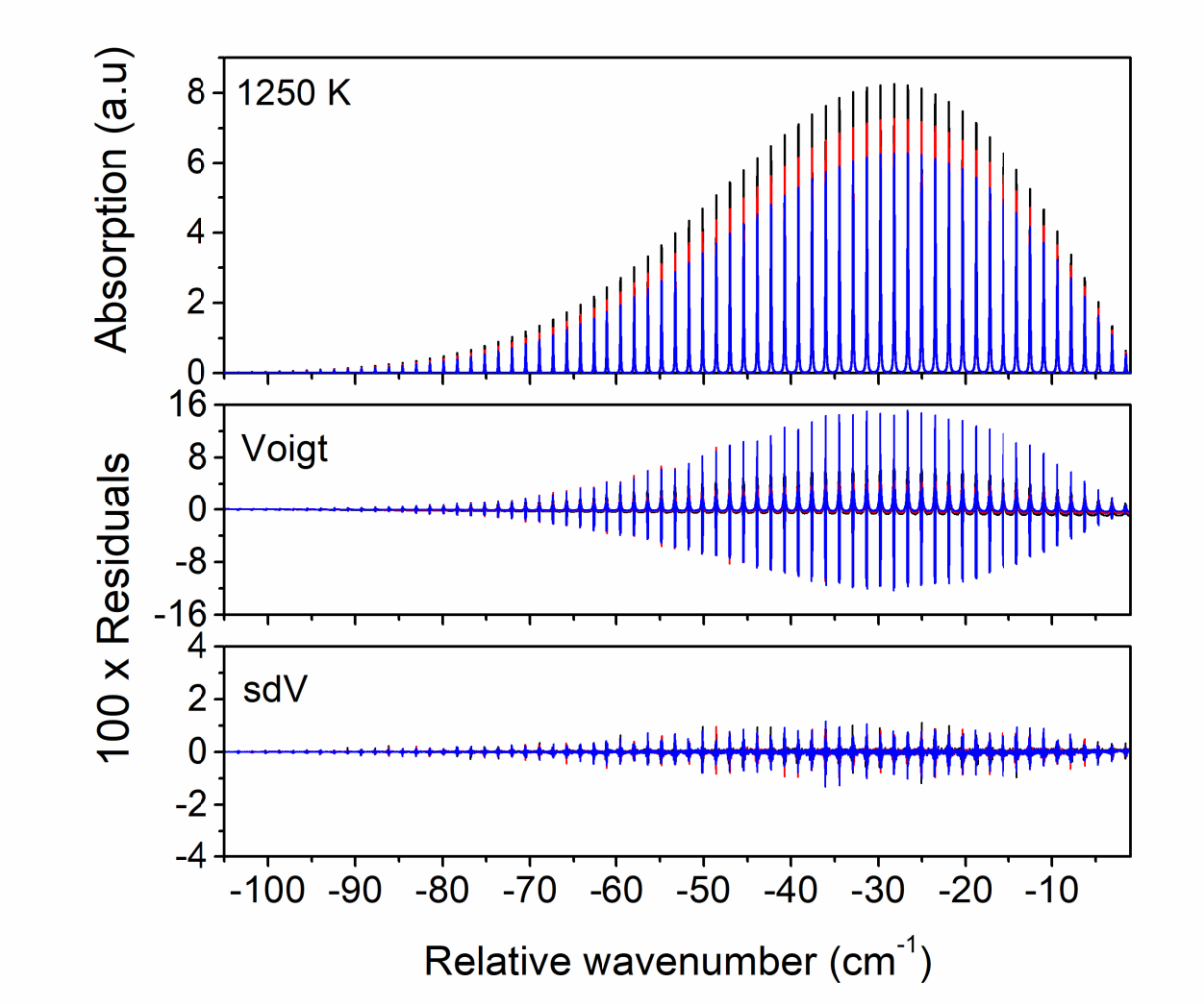

Figure 2: The same as for Fig. 1 but for three values of the Doppler width of $\Gamma_D = 1.17\ 10^{-2}$, $2.35\ 10^{-2}$ and $3.52\ 10^{-2}$ cm^{-1}, at 1250 K.

3. Results and discussions

The values of γ_0, γ_2 and of ζ obtained from fits of the rCMDS spectra at the five considered temperatures, along with their temperature dependences for the Voigt and the sdV profiles, are presented in the following sub-sections and reported in Tables 1-3. These data, plotted against m (with $m = -J$ in the P branch) will be compared with the corresponding values from the HITRAN database and with available experimental data. The reported uncertainty for each parameter includes both the statistical uncertainty obtained from the fits and the difference observed when fitting the entire P branch versus fitting smaller microwindows of 3-4 cm^{-1}.

3.1 Voigt broadening coefficients and their temperature dependence

Figure 3 shows the values of γ_0 obtained with the Voigt profile at room temperature. For lines with $J < 60$, the line broadening coefficients were directly retrieved from the rCMDS spectra computed at 296 K. For higher J values, γ_0 was deduced from the line broadening parameters retrieved at higher temperature and using the single power law. This is thus interesting to compare our values with the extrapolation used in HITRAN for these high J lines.

As observed in Fig. 3, there is a good agreement between our predicted values and the plotted measured data, as well as with the HITRAN values, for the entire considered range of m. The averaged differences between the rCMDS values and the experimental data of Ref. [30] for the $3\nu_1 + \nu_3$ bands, of Ref. [11] for the ν_3 band, and of Ref. [16] for the $3\nu_3$ band, are respectively 2.4 (1.5) %, 2.3 (1.4) % and 3.1 (2.4) % (the numbers in parenthesis correspond to the standard deviation of the calculated averages). In the high J range, our values also show satisfactory agreement with the empirical extrapolations used in HITRAN [20] and in Ref. [16], with a slightly better match with HITRAN. For $60 \leq J \leq 100$, the averaged differences between the theoretically predicted γ_0 and the HITRAN values is 3.8 (2.5) % while it is 6.3 (1.7) % when comparing rCMDS results with values of Ref. [16].

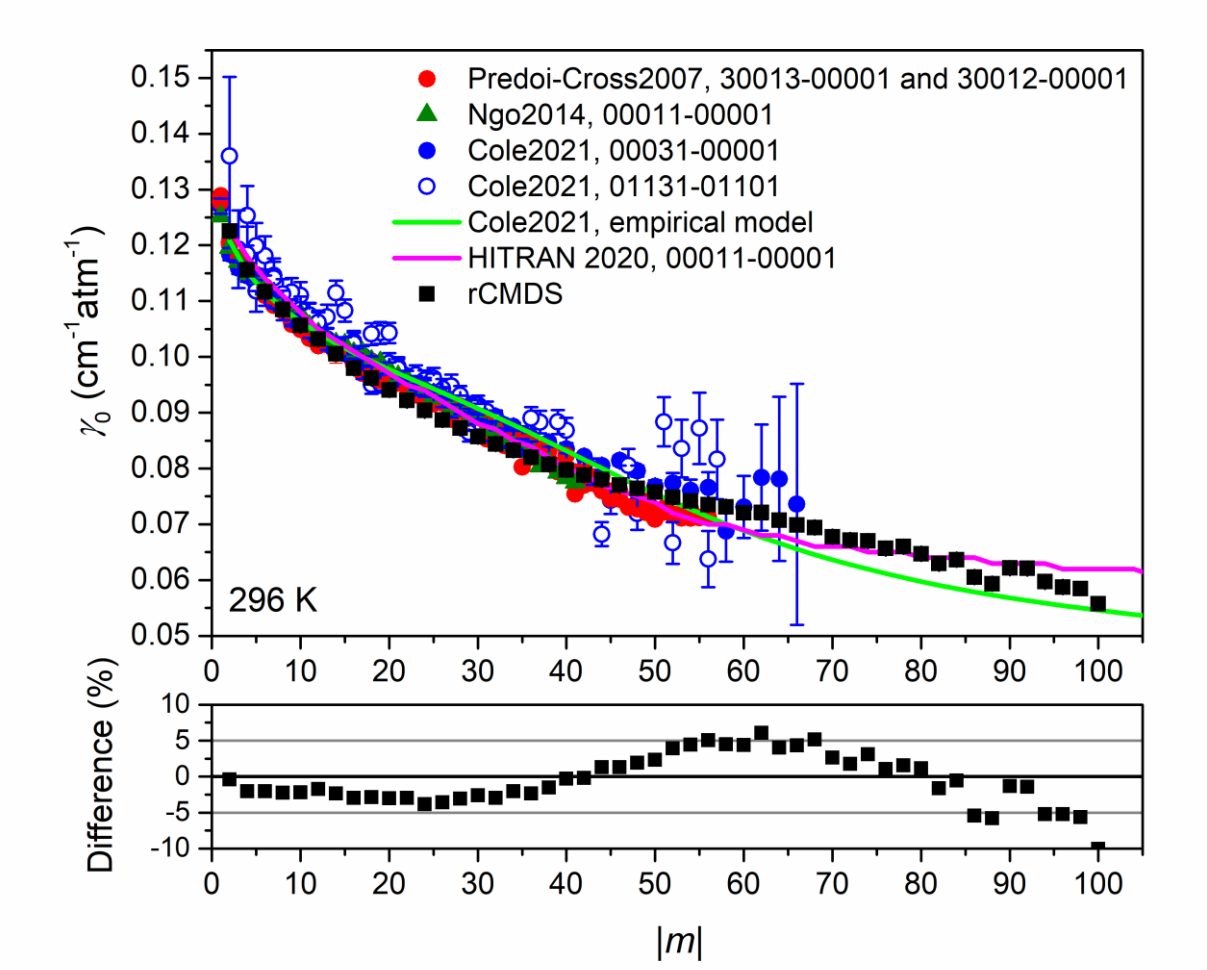

Figure 3: Upper panel: Self-broadening coefficients at 296 K, deduced from fits of rCMDS-calculated spectra with the Voigt profile. The values of γ_0 for high rotational quantum number lines were derived from those obtained at higher temperatures and their temperature dependences (see text for details). These values are compared with data measured at room temperature from Ngo2014 (i.e. Ref. [11]), Cole2021 (i.e. Ref. [16]), and Predoi-Cross2007 (i.e. Ref. [30]) for different vibrational bands, as well as with those of the HITRAN database [18] for the ν_3 band. The empirical modeling proposed by Ref. [16] is also displayed. Lower panel: percent difference between the rCMDS-predicted results and HITRAN 2020 values.

In figures 4 and 5, rCMDS-predictions obtained at 500 K, 750 K, 1000 K and 1250 K are compared with measured and modeled values from Ref. [16] and HITRAN 2020 data. In Ref.

[16], γ_0 was measured for the $3\nu_3$ and $\nu_2 + 3\nu_3 - \nu_2$ bands at 496 K, 737 K, and 980 K. These measured values were corrected using the temperature dependence exponent provided in Ref. [16] (see Fig 5 of Ref. [16]) in order to compare with rCMDS results at 500 K, 750 K and 1000 K.

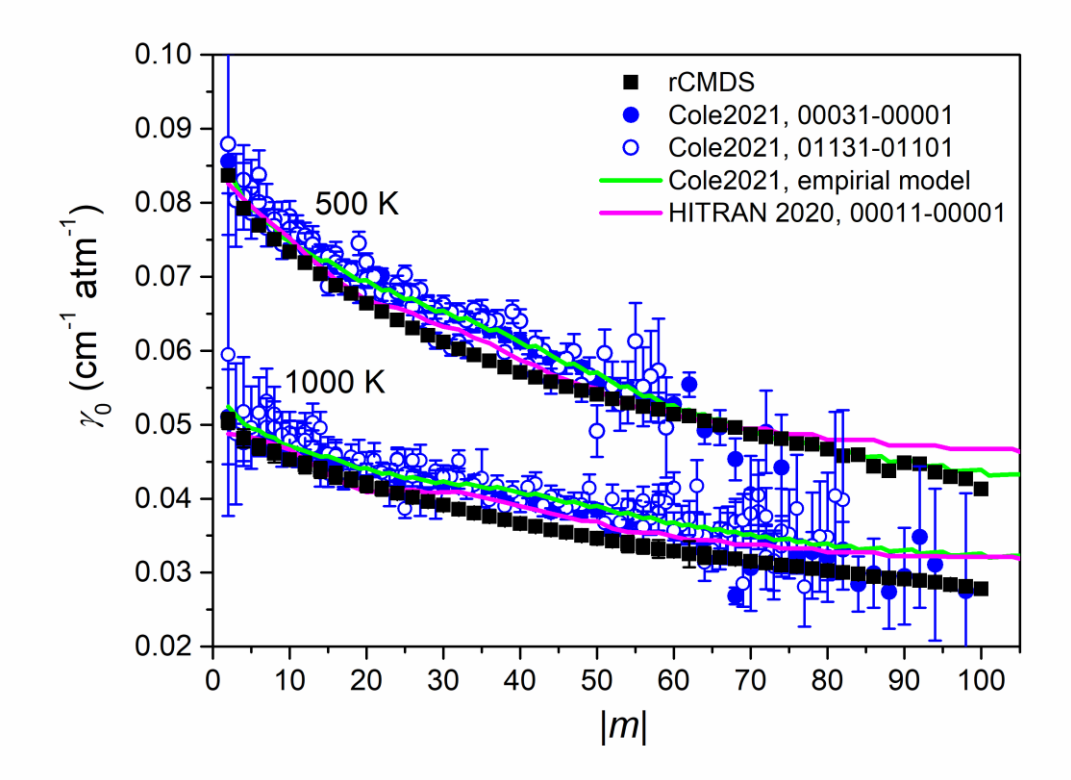

Figure 4: Self-broadening coefficients at 500 K and 1000 K deduced from fits of rCMDS-calculated spectra with the Voigt profile. They are compared with measured values of Cole2021 (Ref. [16]) as well as with the empirical modelings of γ_0 proposed by Ref. [16] and by Ref. [20] for HITRAN 2020.

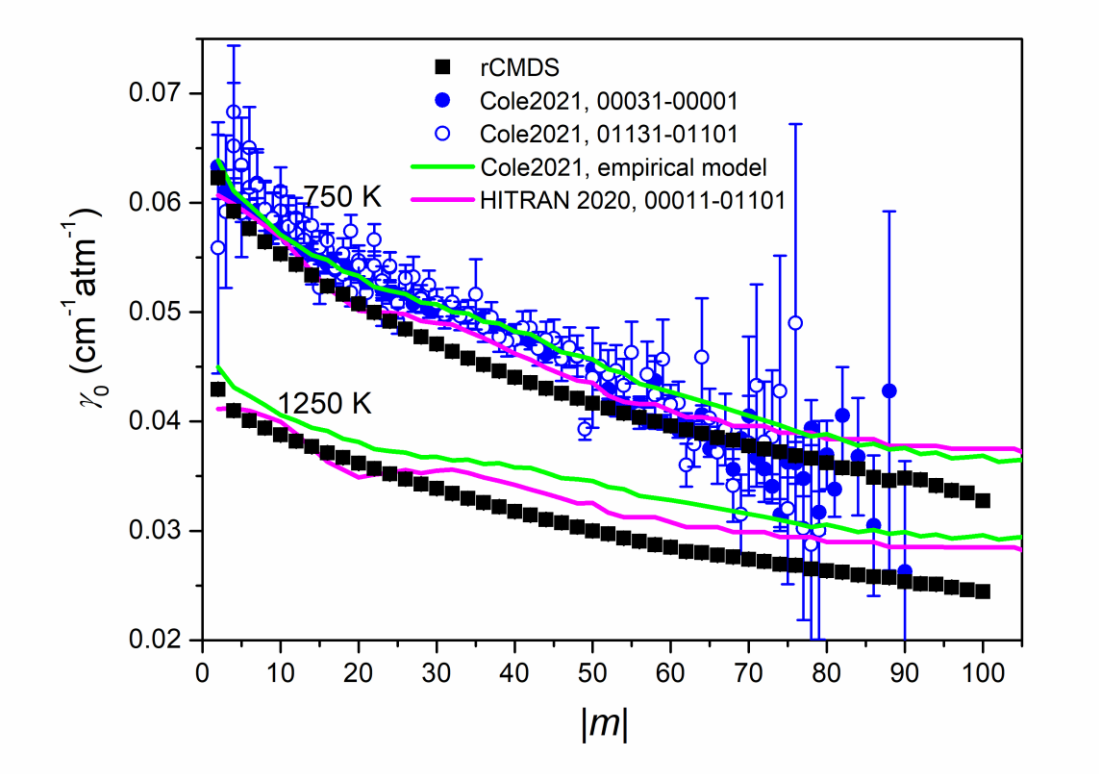

Figure 5: Self-broadening coefficients at 750 K and 1250 K deduced from fits of rCMDS-calculated spectra with the Voigt profile. They are compared with measured values of Cole2021 (Ref. [16]) and with the empirical modelings of γ_0 in Ref. [16] and in HITRAN 2020 [18].

In Ref. [16], an empirical model for γ_0 was deduced by fitting a Padé approximant to the measured values of γ_0 for the $3\nu_3$ band. A similar Padé approximant was used to model the temperature dependence. These models were applied here to deduce the modeled values of γ_0 at the considered temperatures (green curves in Figs. 3-5). The same method was used for calculating HITRAN data (magenta curves). As can be observed, all these values generally agree well with rCMDS predictions, except for the $25 < J < 60$ range, where the rCMDS results are lower than the modeled values of HITRAN 2020, which, in turn, are lower than the measured and modeled values of Ref. [16]. The discrepancy between rCMDS results and values in Ref. [16], which is devoted to the $3\nu_3$ and $\nu_2 + 3\nu_3 - \nu_2$ bands, can be partly attributed to the vibrational dependence of the collisional width associated with the ν_3 mode. Indeed, in Ref. [14], it was shown that the broadening coefficients measured in the $3\nu_3$ are up to approximately 10% larger than those for the $3\nu_1 + \nu_3$ band. Taking this vibrational dependence into account, we estimate that rCMDS results agree with the measured values of Ref. [16] within 5%. Nevertheless, predicting CO_2 self-broadening within 5% accuracy across a broad range of rotational quantum numbers and temperatures, without any adjustable parameters, represents a valuable accomplishment of this method. Finally, for higher J, rCMDS results show better agreement with the measurements compared to the empirical models. As discussed in Sec. 3.2, we suspect that empirical models may overestimate line broadening coefficients at high temperature for high J lines.

On average, the differences between rCMDS results and the empirical model of Ref. [16] are 3.2(2.2) %, 6.6(1.9) %, 8.9(2.9) % and 10.7(3.9) % at 500 K, 750 K, 1000 K and 1250 K,

respectively. In comparison, the differences between rCMDS values and HITRAN 2020 data are 2.8(2.5) %, 4.5(2.8) %, 5.8 (3.1) % and 6.8(3.5) % at the same temperatures.

The single power law was fitted to the rCMDS-deduced values of γ_0 at various temperatures to determine the temperature dependence exponent n_{γ_0}. Figure 6 presents some examples of the temperature dependence of γ_0, demonstrating that the single power law is well-suited for the considered temperature range.

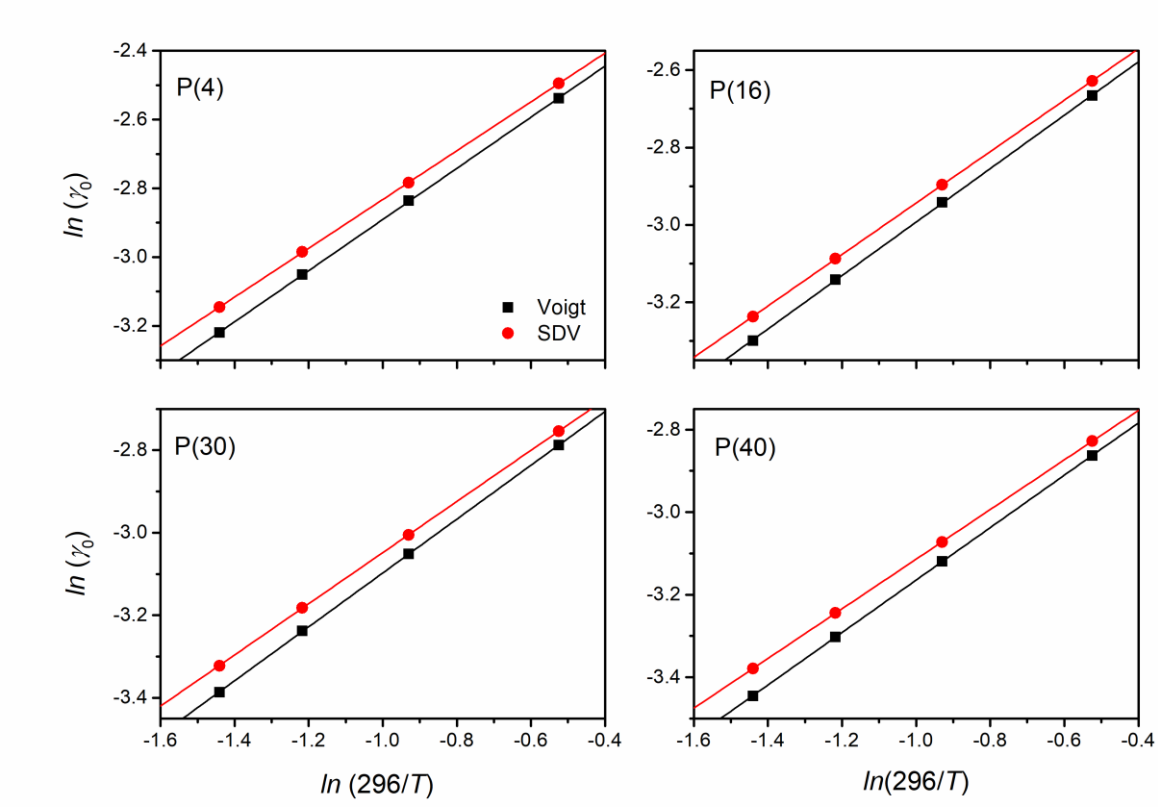

Figure 6: Broadening coefficients versus temperature for several lines, obtained from fits of the rCMDS spectra with the Voigt and SDV profiles, and their fits (straight line) using the single power law.

The obtained values of n_{γ_0} are plotted in Fig. 7, along with data from the HITRAN database [18], and measured values of [8] and [16] for various bands. The Padé approximant from Ref. [16], derived from fits of data measured in the $3\nu_3$ band, is also displayed for comparison. As it can be observed, rCMDS values are in good agreement with measured data for $J < 35$, but notably higher for higher J. While HITRAN data and the model from [16] exhibit peaks around $J = 18$ and $J = 24$, rCMDS values generally decrease monotonously with $|m|$, except for a small peak at $|m| = 60$. Note that experimental values of Ref. [4] are in good agreement with our rCMDS results, both showing higher values of n_{γ_0} at high J, thus leading to larger line broadening coefficients at high temperature, with respect to the empirical models of [16] and HITRAN.

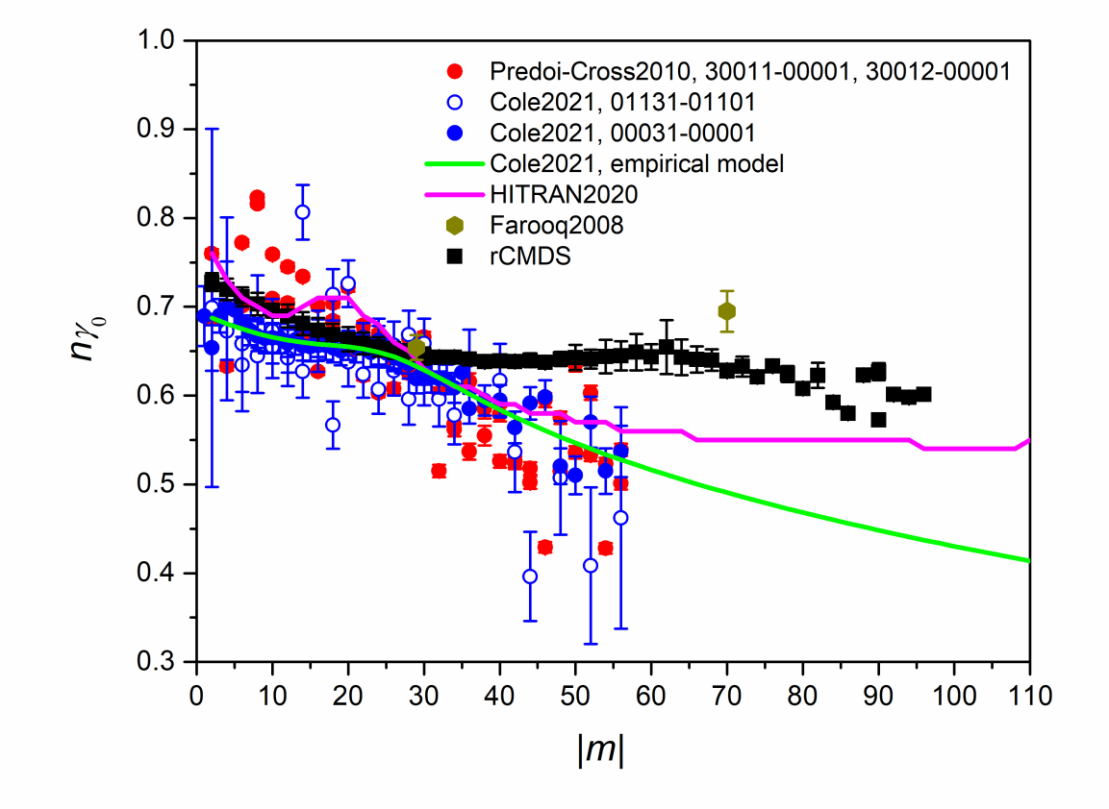

Figure 7: The temperature dependence exponent of the Voigt broadening coefficient, n_{γ_0}, obtained from rCMDS and comparison with measured values of Predoi-Cross2010 (Ref. [8]) and Farooq2008 (Ref. [4]) for various bands, as well as with values provided in HITRAN 2020 [18]. The empirical model of Cole2021 (Ref. [16]) is also plotted for comparison.

3.2 Speed dependent Voigt broadening coefficients and their temperature dependence

Figure 8 presents the room temperature sdV broadening coefficients obtained from the rCMDS spectra. As with the Voigt broadening coefficients, values of γ_0 for high J lines at room temperature were deduced from those retrieved at high temperature spectra and using the single power law. The rCMDS results are compared with experimental results of Ref. [12] for the $3\nu_1 + \nu_3$ band, Ref. [16] for the $3\nu_3$ band, and Ref. [14] for the $3\nu_1 + \nu_3$ and $3\nu_3$ bands. All these experimental data were obtained with the use of the sdV profile. In Ref. [14], line broadening coefficients measured for $3\nu_3$ band are notably larger than those for the $3\nu_1 + \nu_3$ band. Measurements from Ref. [16] for the same $3\nu_3$ band are in very good agreement with those of Ref. [14]. The discrepancy between the line broadening coefficients measured for the $3\nu_3$ and those of the other bands has been attributed to the vibrational dependence of the line width associated with the ν_3 mode. Consequently, HITRAN 2020 used measured data for the $3\nu_1 + \nu_3$ band from Ref. [14] to derive line broadening coefficients for all bands with smaller vibrational quanta. As a result, HITRAN data are smaller compared to the empirical model from [16], which was derived from fits to measured values in the $3\nu_3$ band (the magenta and green curves in Fig. 8). We can observe that rCMDS predictions are in very good agreement with measured values from Ref. [14] for the $3\nu_1 + \nu_3$ band, with an average difference of 3(4) %, and thus also with HITRAN data. However, for $|m| > 64$, HITRAN data appear to overestimate both the measured and rCMDS values, while the rCMDS results show very good agreement with the empirical model from [16].

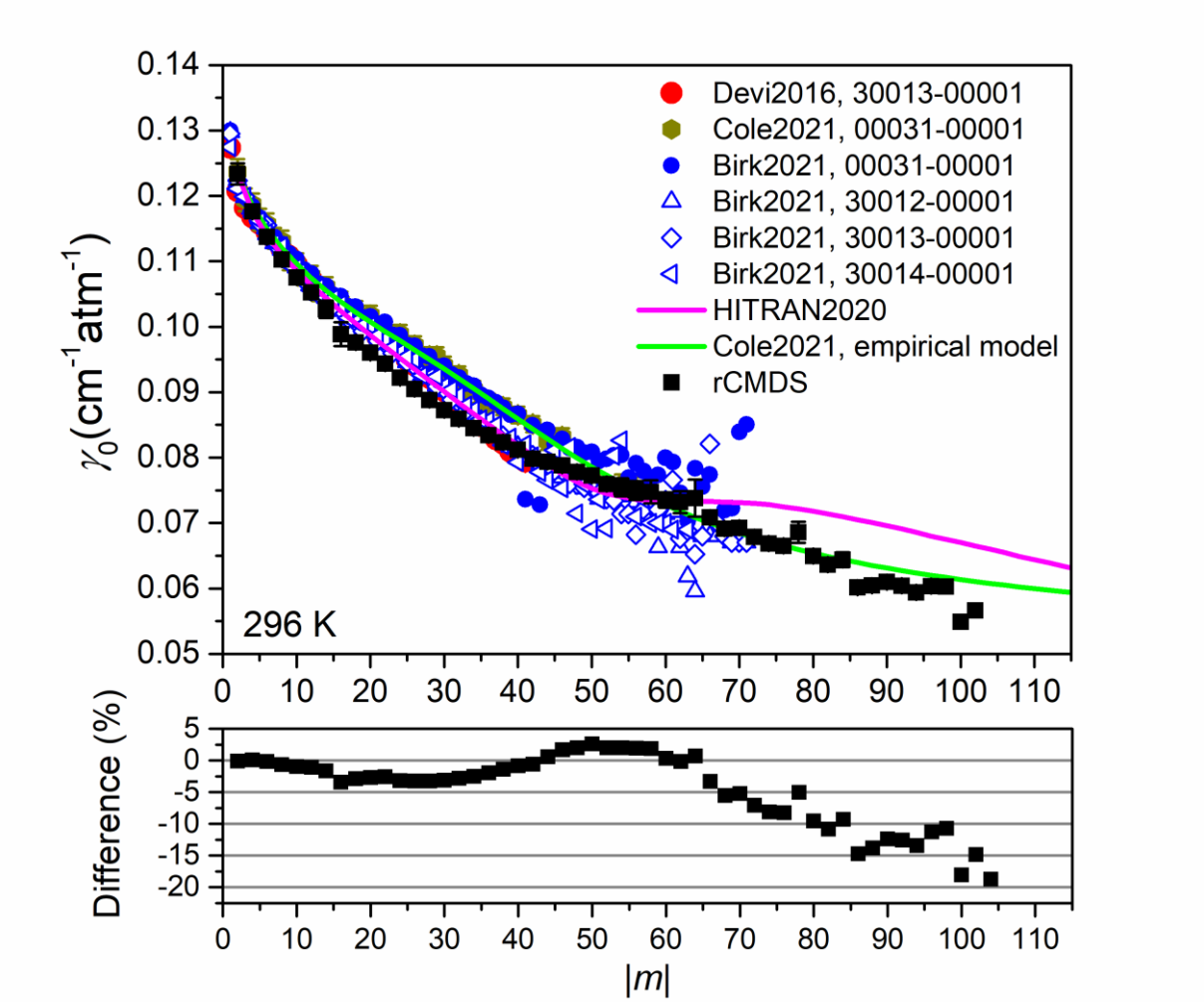

Figure 8: Upper panel: Self-broadening coefficients of CO_2 lines at 296 K, obtained from fits of rCMDS-spectra using the sdV profile. For high rotational quantum numbers, the values of γ_0 were deduced from those retrieved at higher temperatures (see text for details). These values are compared with room temperature measured values from Devi2016 (Ref. [12]), Birk2021 (Ref. [14]), and Cole2021 (Ref. [16]) for various vibrational bands, and with HITRAN 2020 data [18] for the ν_3 band. The empirical model of Ref. [16] is also displayed for comparison. Lower panel: percent difference between the rCMDS-predicted results and HITRAN 2020 values.

Figure 9 shows a comparison of rCMDS predictions at 1000 K with values from the HITRAN database, as well as from Refs. [12] and [16] for the same temperature. The temperature dependence in HITRAN is derived from [12], which explains the very good agreement observed between HITRAN and [12] in this figure. However, HITRAN values are significantly lower than rCMDS results and data from Ref. [16] for $|m| < 54$. On the opposite, for higher values of $|m|$, HITRAN data are substantially larger than both rCMDS predictions and results of Ref. [16]. This is due to the extrapolation for high J lines and to the temperature dependence exponent used in HITRAN. Similar trends are observed at other temperatures (500 K, 750 K and 1250 K). Note that while there is a very good agreement between the empirical model of [16] and rCMDS results at room temperature for the entire range of rotational quantum number considered (Fig. 8), at 1000 K, the empirical model shows significantly higher broadening coefficients at high $|m|$ (Fig. 9), which cannot be totally explained by the vibrational dependence of the line broadening. The modeled

broadening coefficients at 1000 K from Ref. [16] (green curve in Fig. 9), were determined using a single power law and Padé approximants for γ_0 (296 K) and n_{γ_0}, as given in Ref. [16]. However, the Padé approximant for n_{γ_0} was fitted using measured data up to $J = 56$ only (see [16] and Fig. 10). Extrapolation of n_{γ_0} to much higher J values can lead to unphysical results, as illustrated in the insert of Fig. 9. This insert shows broadening coefficients at 1000 K computed from the Padé approximants of Ref. [16] for J between 80 and 240, revealing a decrease in γ_0 until reaching a minimum value of 0.03324 cm^{-1}/atm at $J = 128$, followed by an increase with further J values. This behavior is contrary to what is expected for line broadening of a system such like CO_2, where broadening should decrease with increasing J and approach a constant value due to the negligible rotational contribution compared to vibrational effects. These observations suggest that the broadening coefficients computed from the empirical models of [16] may be inaccurate at high J, explaining the discrepancy between the empirical model and our rCMDS predictions at high J.

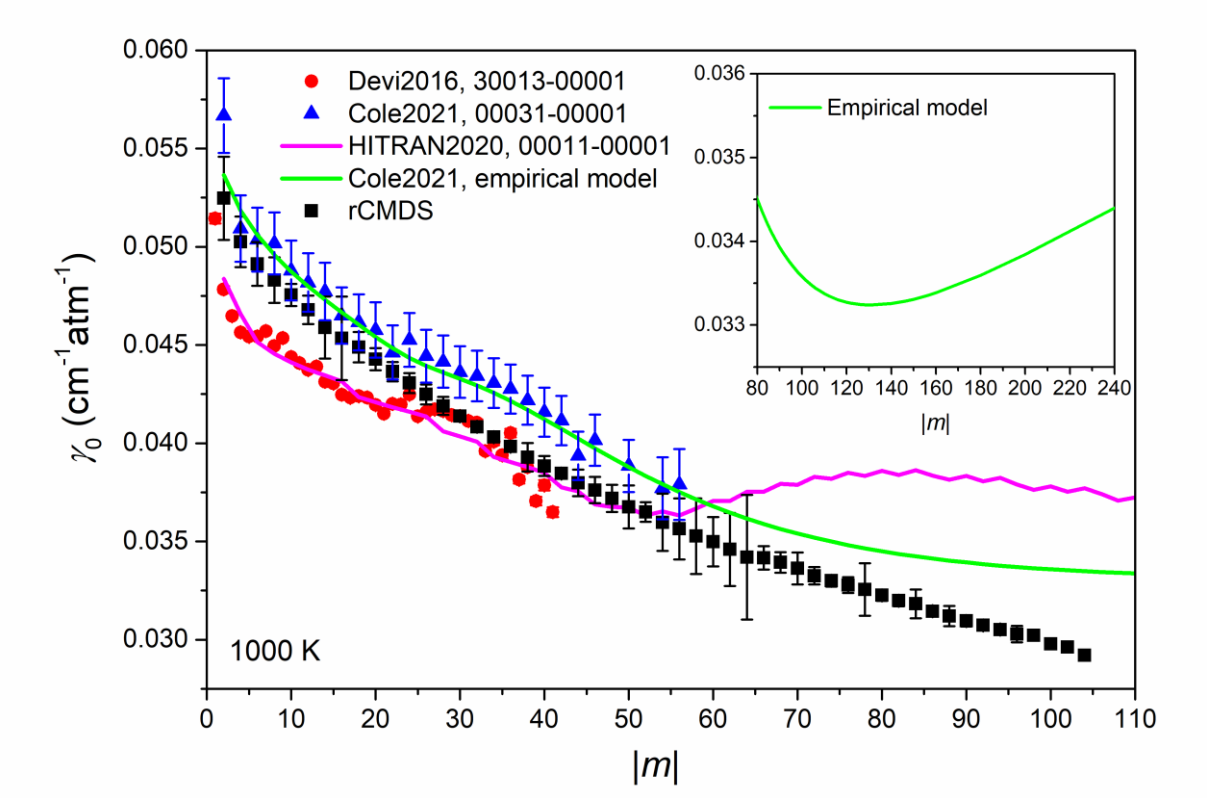

Figure 9: Self-broadening coefficients for CO_2 lines, retrieved from fits of rCMDS spectra using the sdV profile at 1000 K. They are compared with values computed from room temperature measured data of Devi2016 (Ref. [12]) and Cole2021 (Ref. [16]) and the temperature dependence provided in these references. HITRAN values and those obtained using the empirical model of [16] are also displayed for comparison.

The temperature dependence of the sdV broadenings within the considered temperature range is well described by a single power law, as illustrated in Fig. 6. Figure 10 presents the temperature dependence exponents obtained from rCMDS and compares them with HITRAN 2020 data for the ν_3 band, as well as with measured values and the empirical model of Ref. [16] for the $3\nu_3$ band. A very good agreement is observed between rCMDS results and those of [16] for $|m| < 54$. For higher values of $|m|$, the n_{γ_0} values predicted by rCMDS are larger

than the empirical model of [16]. It is important to exercise caution when using empirical laws to extrapolate unmeasured values at high J, as this can lead to unphysically-based results, as shown in Fig. 9. Finally, the n_{γ_0} values from HITRAN show significant discrepancies compared to both rCMDS predictions and results of Ref. [16], which could lead to substantial differences in line broadening coefficients at high temperature (see Fig. 9 for example). We therefore recommend updating the sdV data in the HITRAN database, for γ_0 and its temperature dependence, incorporating both high-quality measured data and the rCMDS results.

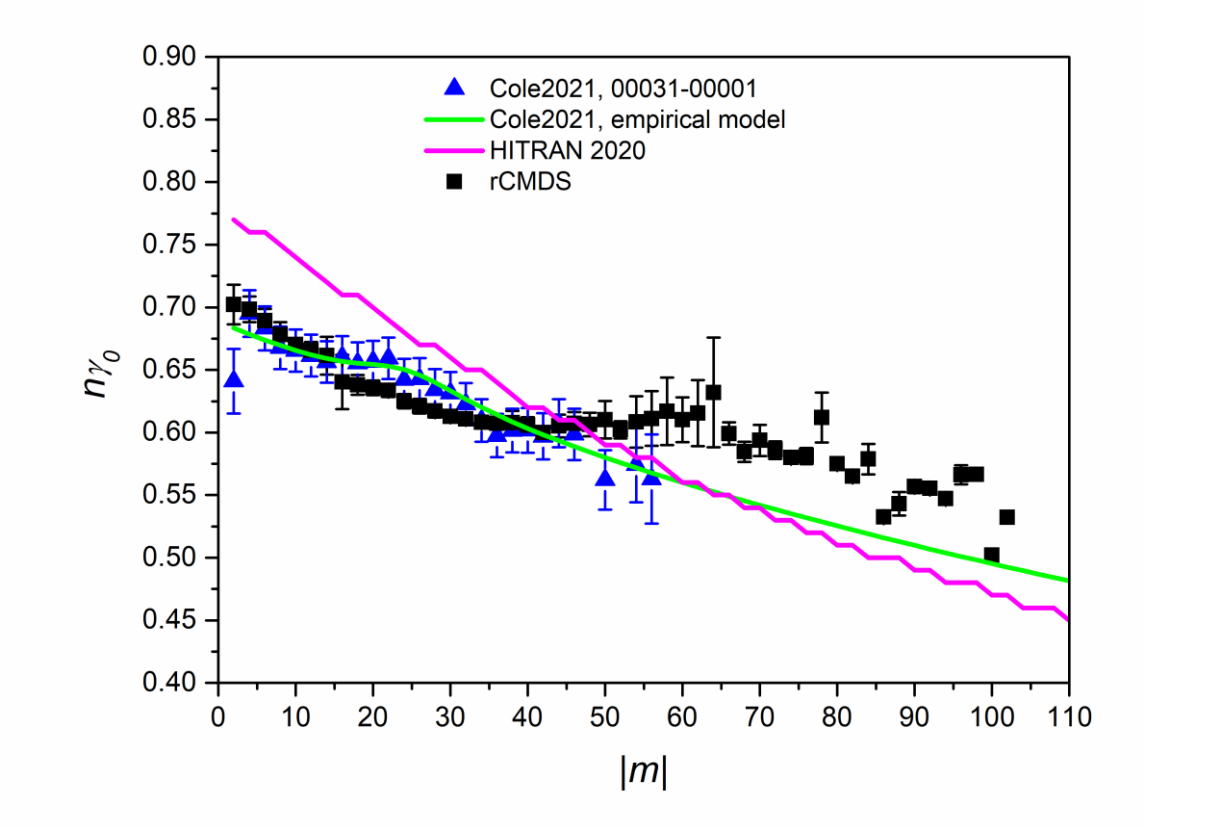

Figure 10: Temperature dependence of the line width, obtained with the sdV profile and comparison with available data.

3.3 Speed dependence of the line width and temperature dependence

The rCMDS results for the speed dependence of the line width are presented in Fig. 11, along with measured values from Refs. [12], [14] and [16]. The results from Birk et al [14] show no vibrational dependence for γ_2, unlike γ_0. The measured values of Ref. [16] are systematically larger than those of Ref. [14], while those of Ref. [12] are systematically smaller. There is an excellent agreement between the rCMDS results and those of Ref. [14]. Since the HITRAN 2020 data are obtained by fitting a Padé approximant to the data of Ref. [14], they also show good agreement with the rCMDS predictions.

rCMDS values of γ_2, obtained at various temperatures, were then used to determine the temperature dependence exponent n_{γ_2}. It is worth noting that many studies assume the temperature dependence of γ_2 to be the same as that of γ_0. However, Winzewsky et al [31] observed that n_{γ_2} is significantly smaller than n_{γ_0} for N_2-broadened CO_2 lines. This finding was then confirmed by our rCMDS predictions for the same system [21]. The same behavior

is observed here for self-broadened CO_2, as shown in Fig. 12, which highlights significant differences between n_{γ_2} and n_{γ_0}. In the HITRAN database [18], n_{γ_2} is not provided, likely due to the lack of available data. In Ref. [16], n_{γ_2} was assumed to be the same as n_{γ_0}.

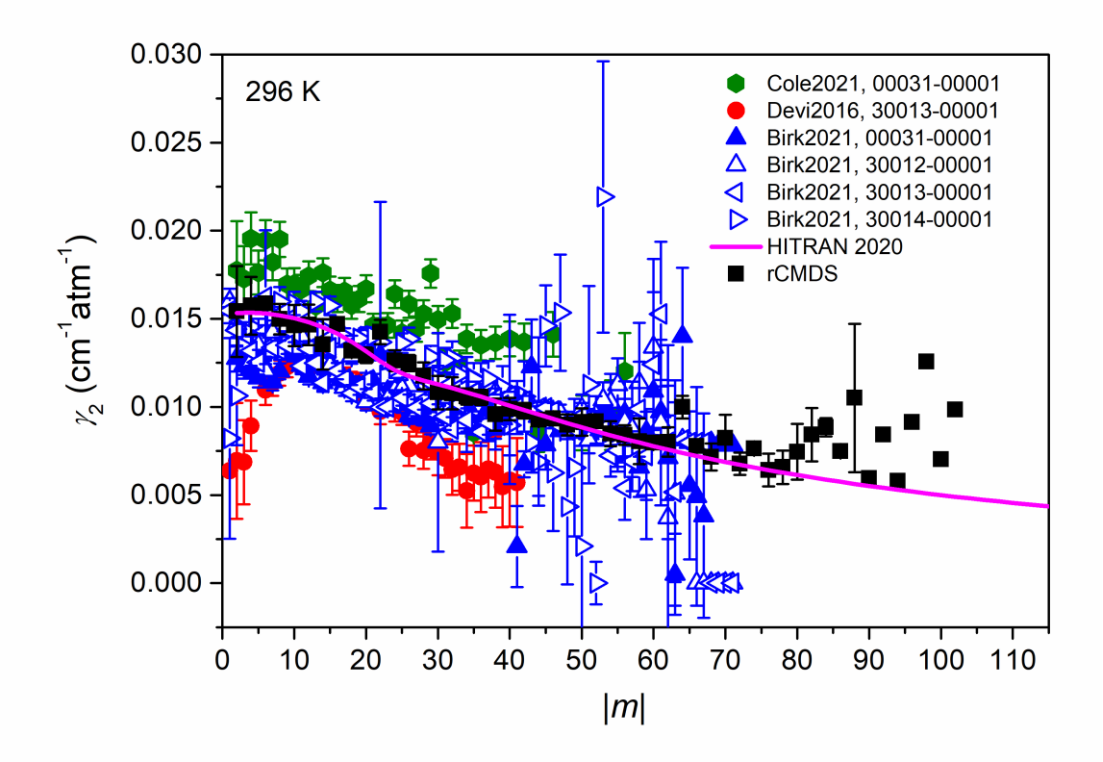

Figure 11: The quadratic speed dependence component of the line width, γ_2, obtained at 296 K from fits of the rCMDS spectra using the sdV profile, and comparisons with experimental values of Devi2016 (Ref. [12]), Birk2021 (Ref. [14]), and Cole2021 (Ref. [16]) for various bands, as well as with HITRAN 2020 data.

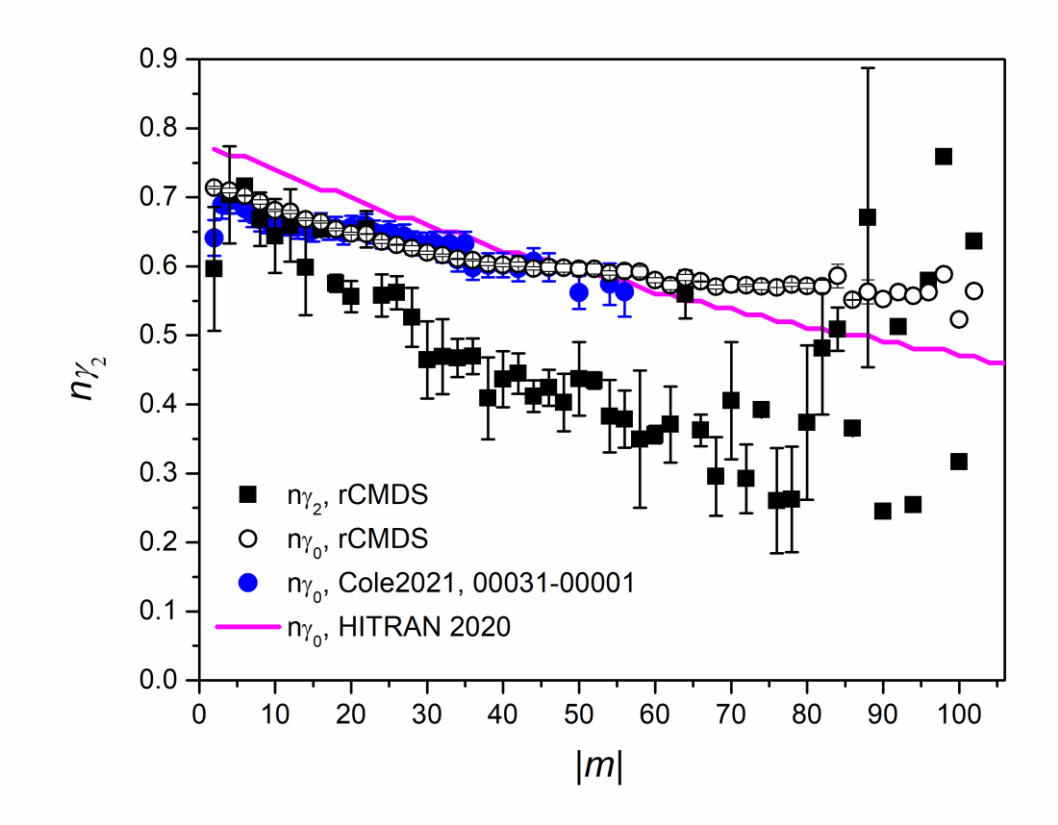

Figure 12: The temperature dependence of the speed dependence component of the line width, n_{γ_2}, obtained from rCMDS and comparison with that of the line width n_{γ_0}.

3.4 First-order line-mixing parameter and its temperature dependence

Since the rCMDS were conducted at 1 atm, only the first-order line-mixing (LM) parameter, applicable in the weak LM regime, could be retrieved from the predicted spectra. At higher densities, where LM effects become significant, taking into account the full relaxation matrix is necessary for accurate modeling of the absorption spectra [32]. In this study, the first-order LM coefficient, ζ, was retrieved from the rCMDS spectra with both the Voigt and sdV profiles for each considered temperature. Several studies have demonstrated that the choice of line shape model does not influence the retrieved LM coefficient (e.g. [21,23,30]), a finding that is also observed here. The obtained LM coefficients are presented in Fig. 13 and compared with experimental values of Refs. [8] and [14], measured at room temperature, as well as with HITRAN 2020 data. The rCMDS-predicted values are in good agreement with the measured data from Ref. [8] and with the HITRAN 2020 data, both of which are smaller than those of Ref. [14], especially for small rotational quantum numbers.

For the temperature dependence of ζ, we noted that for several lines, the sign of the value of ζ can be changed with temperature. The single power law cannot authorize this sign change and thus is not used here. For most lines, it was impossible to fit the data with the complete form of double power law [29] as either the fit cannot be converged or the retrieved results strongly depend on the initial guess of the parameters. We therefore used a simplified form of the double power law, i.e.: $\zeta(T) = A(\frac{T_0}{T})^n + B$. This model thus allows for sign change with temperature. In addition, obtained results showed that this model reproduces very well the

temperature dependence of the predicted values of ζ, as exemplified in Fig. 14. The retrieved data for A, B and n are listed in Table 3.

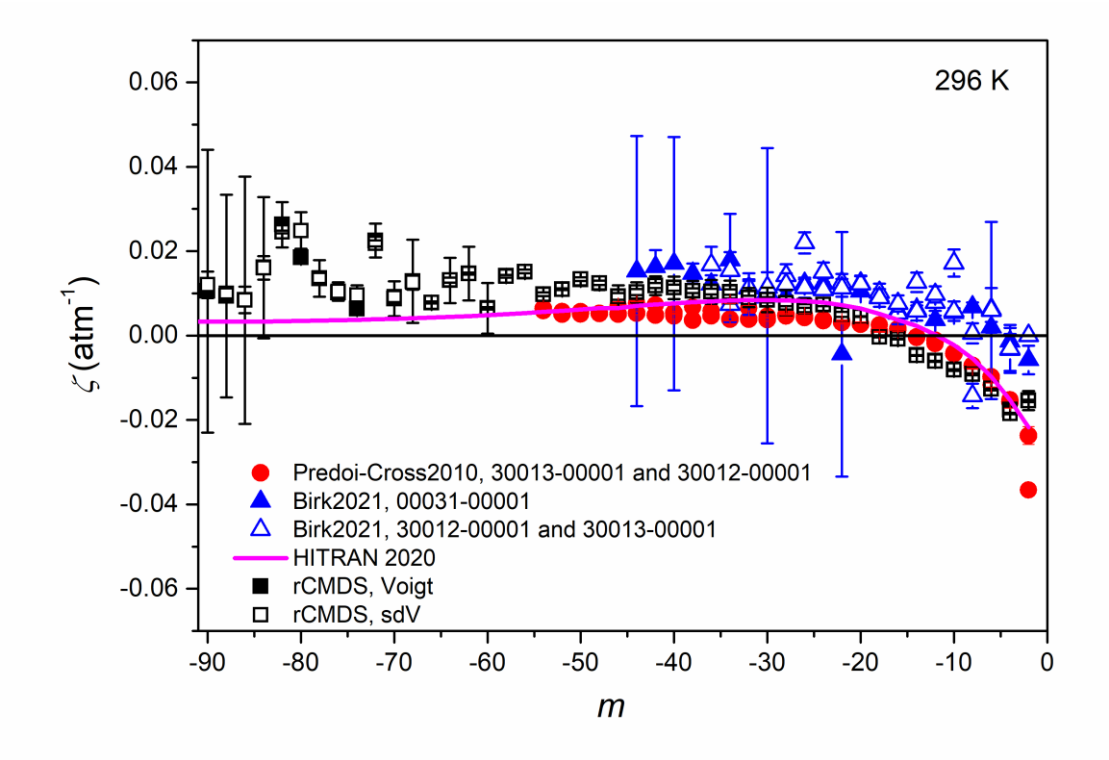

Figure 13: Room temperature first-order line-mixing coefficients obtained from rCMDS and comparison with measured data of Predoi-Cross2010 (Ref. [8]) and Birk2021 (Ref. [14]). Values of the HITRAN 2020 database are also plotted.

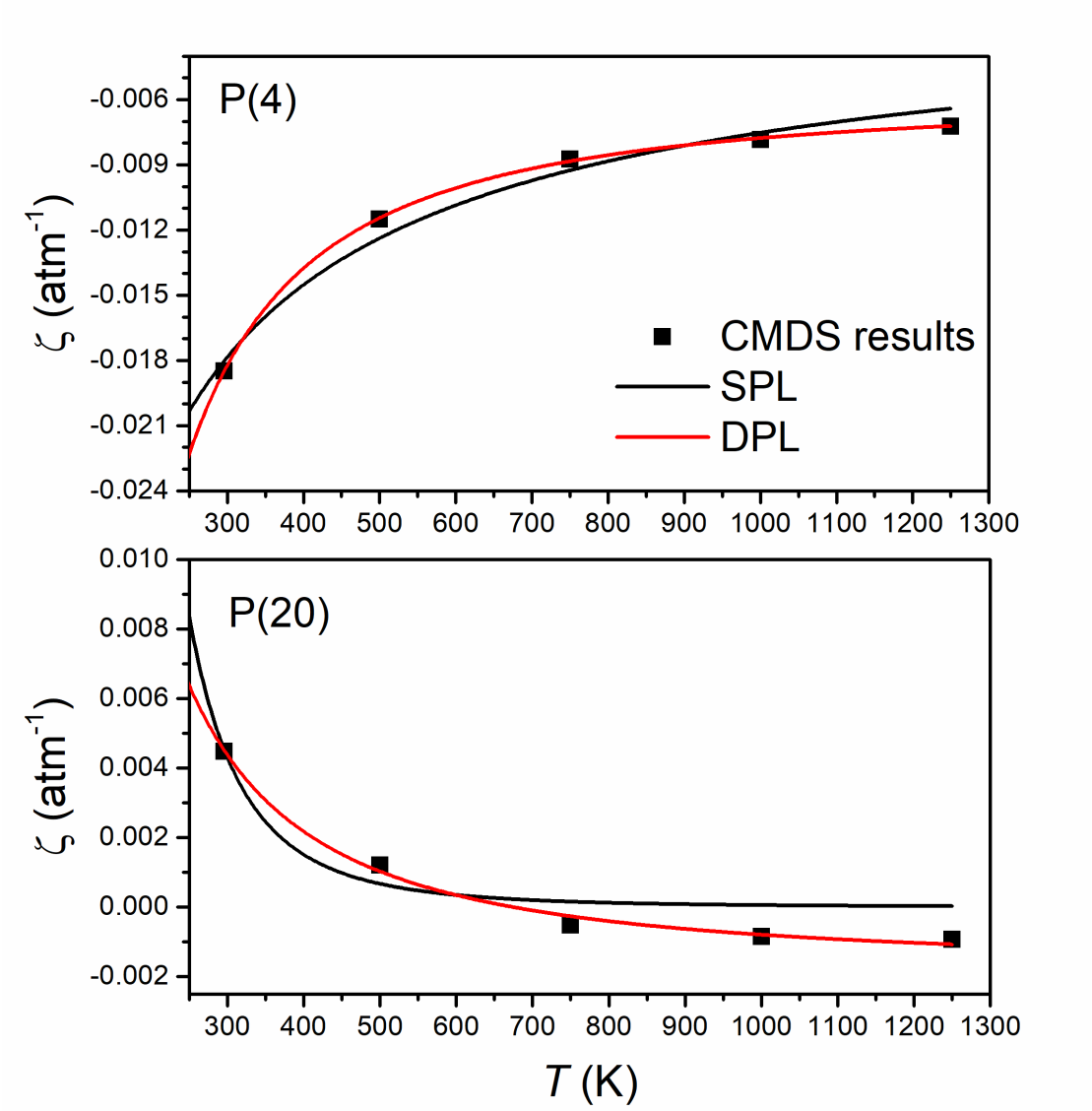

Figure 14: First-order line-mixing coefficient versus temperature for the P(4) and P(20 lines, obtained from rCMDS spectra with the sdV, and their fits with the single power law (SPL) and double power law (DPL).

4. Conclusions

High temperature line-shape parameter data for pure CO_2 are important for various applications including studies of Venus atmosphere and combustion media. While there are many papers devoted to self-broadened CO_2 line shapes at room temperature or at temperatures of the earth atmosphere, few studies address high-temperature conditions. In this study, we employed requantized classical molecular dynamics simulations to predict line-shape parameters of pure CO_2 across a wide temperature range, from 296 K to 1250 K. We predicted line broadening, its speed dependence component and the first-order line-mixing coefficients for rotational quantum numbers up to 100. The obtained parameters and their temperature dependences are compared with data of the HITRAN database [18] and recent experimental studies. These comparisons demonstrate that rCMDS predictions are in very good agreement (e.g. within 5% for the line broadening) with high quality measurements at

both room and high temperature conditions. They also indicate that several parameters in the HITRAN database need to be updated in order to more accurately simulate the absorption spectra of self-broadened CO_2 at high temperatures.

Line	$\boldsymbol{\gamma_0(296\ K)}$	$\boldsymbol{n_{\gamma_0}}$	$\boldsymbol{\zeta\ (296\ K)}$
P(2)	0.1225(6)	0.728(10)	-0.0154(23)
P(4)	0.1156(7)	0.720(12)	-0.0176(11)
P(6)	0.1117(6)	0.711(11)	-0.0126(7)
P(8)	0.1085(7)	0.703(13)	-0.0091(5)
P(10)	0.1056(4)	0.696(8)	-0.0080(4)
P(12)	0.1032(7)	0.690(13)	-0.0060(2)
P(14)	0.1006(7)	0.680(13)	-0.0046(4)
P(16)	0.0980(7)	0.673(14)	-0.0008(2)
P(18)	0.0962(6)	0.669(12)	--
P(20)	0.0941(7)	0.663(14)	0.0044(1)
P(22)	0.0922(6)	0.659(12)	0.0050(5)
P(24)	0.0904(5)	0.655(11)	0.0073(9)
P(26)	0.0887(5)	0.651(9)	0.0070(19)
P(28)	0.0872(4)	0.648(9)	0.0077(31)
P(30)	0.0857(5)	0.644(10)	0.0084(29)
P(32)	0.0844(3)	0.643(7)	0.0090(23)
P(34)	0.0833(2)	0.643(3)	0.0103(27)
P(36)	0.0820(2)	0.641(4)	0.0104(28)
P(38)	0.0808(1)	0.638(2)	0.0105(24)
P(40)	0.0797(1)	0.639(3)	0.0113(27)
P(42)	0.0788(1)	0.638(2)	0.0118(22)
P(44)	0.0780(1)	0.640(8)	0.0102(24)
P(46)	0.0770(2)	0.637(3)	0.0093(26)
P(48)	0.0764(4)	0.641(8)	0.0124(16)
P(50)	0.0757(6)	0.643(14)	0.0133(13)
P(52)	0.0748(5)	0.641(11)	0.0110(6)
P(54)	0.0742(8)	0.644(19)	0.0098(9)
P(56)	0.0735(7)	0.645(16)	0.0151(11)
P(58)	0.0731(9)	0.649(21)	0.0141(4)
P(60)	0.0720(6)	0.644(14)	0.0065(6)
P(62)	0.0721(12)	0.655(30)	0.0147(6)
P(64)	0.0707(8)	0.643(20)	0.0131(5)
P(66)	0.0699(6)	0.641(15)	0.0077(10)
P(68)	0.0694(7)	0.640(12)	0.0129(10)
P(70)	0.0678(4)	0.628(7)	0.0087(41)
P(72)	0.0672(9)	0.627(11)	0.0225(40)
P(74)	0.0670(6)	0.633(6)	0.0063(6)
P(76)	0.0657(2)	0.621(7)	0.0102(14)
P(78)	0.0660(3)	0.633(9)	0.0135(43)
P(80)	0.0647(5)	0.624 (2)	0.0185(2)
P(82)	0.0630(6)	0.608(14)	0.0263(54)
P(84)	0.0636(9)	0.623(5)	0.0161(17)
P(86)	0.0605(3)	0.592(4)	0.0084(29)

P(88)	0.0593(3)	0.580(6)	0.0094(240)
P(90)	0.0622(4)	0.623(10)	0.0105(34)
P(92)	0.0621(6)	0.627(6)	--
P(94)	0.0597(4)	0.601(4)	0.0040(27)
P(96)	0.0588(3)	0.598(7)	0.0051(39)
P(98)	0.0585	0.601	
P(100)	0.0558	0.572	

Table 1: CO_2 self-broadening coefficients at 296 K, γ_0 (cm^{-1} atm^{-1}), the temperature dependence exponents for the line broadening, n_{γ_0}, and the first-order line-mixing coefficients at 296 K, ζ (atm^{-1}), obtained from rCMDS spectra with the Voigt profile. The uncertainties given in parenthesis are multiples of the last significant digit.

Line	$\boldsymbol{\gamma_0(296\ K)}$	$\boldsymbol{n_{\gamma_0}}$	$\boldsymbol{\gamma_2(296\ K)}$	$\boldsymbol{n_{\gamma_2}}$	$\boldsymbol{\zeta\ (296\ K)}$
P(2)	0.1234 (3)	0.702(4)	13.8(8)	0.710(65)	-0.0155(3)
P(4)	0.1176(2)	0.698(3)	11.3(4)	0.459(50)	-0.0185(2)
P(6)	0.1137(2)	0.689(2)	11.4(4)	0.459(47)	-0.0127(3)
P(8)	0.1103(2)	0.678(3)	10.6(4)	0.393(47)	-0.0092(3)
P(10)	0.1075(1)	0.670(1)	10.7(3)	0.398(39)	-0.0081(2)
P(12)	0.1052(1)	0.666(2)	11.1(3)	0.439(30)	-0.0061(1)
P(14)	0.1027(3)	0.661(4)	11.0(2)	0.438(18)	-0.0047(7)
P(16)	0.0989(4)	0.640(5)	11.6(1)	0.503(7)	-0.0008(1)
P(18)	0.0976(1)	0.638(2)	9.1(3)	0.279(44)	-0.0004(1)
P(20)	0.0960(1)	0.636(2)	10.4(2)	0.388(21)	0.0045(1)
P(22)	0.0944(1)	0.633(2)	11.0(2)	0.447(20)	0.0050(6)
P(24)	0.0922(1)	0.625(2)	9.8(3)	0.350(32)	0.0074(4)
P(26)	0.0905(1)	0.621(2)	9.7(3)	0.350(37)	0.0070(4)
P(28)	0.0888(1)	0.617(2)	9.1(3)	0.313(35)	0.0077(8)
P(30)	0.0873(1)	0.612(1)	8.8(2)	0.298(26)	0.0085(6)
P(32)	0.0859(1)	0.611(1)	8.7(2)	0.290(32)	0.0090(5)
P(34)	0.0845(1)	0.608(1)	7.8(3)	0.213(47)	0.0103(6)
P(36)	0.0834(1)	0.607(1)	8.2(3)	0.265(36)	0.0104(7)
P(38)	0.0823(2)	0.608(3)	8.7(1)	0.343(13)	0.0106(6)
P(40)	0.0812(1)	0.606(2)	8.2(2)	0.290(25)	0.0113(7)
P(42)	0.798(1)	0.6001)	6.8(4)	0.132(66)	0.0119(6)
P(44)	0.794(1)	0.605(2)	7.9(2)	0.269(32)	0.0103(7)
P(46)	0.788(1)	0.607(2)	9.0(1)	0.391(10)	0.0093(8)
P(48)	0.778(1)	0.606(3)	7.9(2)	0.279(31)	0.0125(5)
P(50)	0.0773(2)	0.610(4)	8.2(2)	0.331(26)	0.0134(4)
P(52)	0.0760(1)	0.602(2)	7.1(4)	0.188(62)	0.0110(2)
P(54)	0.0755(3)	0.608(5)	7.5(1)	0.275(20)	0.0098(4)
P(56)	0.0750(3)	0.611(6)	7.9(1)	0.329(9)	0.0152(4)
P(58)	0.0748(4)	0.617(8)	8.3(2)	0.382(26)	0.0141(4)
P(60)	0.0735(3)	0.610(5)	8.4(1)	0.395(5)	0.0065(3)
P(62)	0.0732(4)	0.616(7)	6.6(2)	0.196(41)	0.0147(3)
P(64)	0.0738(6)	0.632(11)	11.8(7)	0.768(100)	0.0131(6)
P(66)	0.0709(2)	0.599(3)	6.2(5)	0.140(95)	0.0079(2)
P(68)	0.0691(2)	0.585(2)	5.6(2)	0.091(29)	0.0126(18)

P(70)	0.0693(2)	0.594(3)	9.1(2)	0.487(15)	0.0092(13)
P(72)	0.0679(2)	0.586(2)	7.1(1)	0.336(9)	0.0219(7)
P(74)	0.0669(1)	0.580(2)	5.4(2)	0.113(41)	0.0096(22)
P(76)	0.0665(1)	0.581(2)	7.3(1)	0.367(18)	0.0104(22)
P(78)	0.0686(4)	0.612(5)	11.4(6)	0.714(60)	0.0136(12)
P(80)	0.0650(1)	0.575(2)	6.0(1)	0.207(24)	0.0249(43)
P(82)	0.0636(1)	0.565(2)	7.7(1)	0.419(14)	0.0245(4)
P(84)	0.0644(3)	0.579(4)	8.0(1)	0.436(2)	0.0161(28)
P(86)	0.0601(1)	0.532(1)	5.6(1)	0.183(9)	0.0084(31)
P(88)	0.0604(2)	0.543(3)	8.1(3)	0.477(33)	0.0100(12)
P(90)	0.0610(1)	0.557(2)	4.7(1)	0.684(6)	0.0120(31)
P(92)	0.0604(3)	0.555(1)			
P(94)	0.0594(1)	0.547(1)	5.5(1)	0.217(1)	0.0038(36)
P(96)	0.0603(2)	0.567(2)	8.9(1)	0.576(13)	0.0049(31)
P(98)	0.0602	0.566			
P(100)	0.0549	0.502			
P(102)	0.0566	0.532			

Table 2: CO_2 self-broadening coefficients at 296 K, γ_0 (cm^{-1} atm^{-1}), their speed dependence component at 296 K, γ_2 (10^{-3} cm^{-1} atm^{-1}), the temperature dependence exponents for the line broadening, n_{γ_0} and for the speed dependence, n_{γ_2}, and the first-order line-mixing coefficients at 296 K, ζ (atm^{-1}), obtained from rCMDS spectra with the speed dependent Voigt profile. The uncertainties given in parenthesis are multiples of the last significant digit.

Line	$\boldsymbol{A}$	$\boldsymbol{n}$	$\boldsymbol{B}$
P(2)	0.0069(3)	-0.548(32)	-0.223(4) 10^{-1}
P(4)	-0.0126(1)	1.564(18)	-0.590(4) 10^{-2}
P(6)	-0.0148(1)	0.539(8)	0.213(6) 10^{-2}
P(8)	-0.0639(1)	0.062(2)	0.548(1) 10^{-1}
P(10)	-0.0084(2)	0.544(19)	0.260(80) 10^{-3}
P(12)	-0.0104(1)	0.310(12)	0.433(8) 10^{-2}
P(14)	-0.0148(3)	0.140(22)	0.100(3) 10^{-1}
P(16)	-0.0008(2)	0.164(108)	--
P(18)	-0.0004(1)	-0.691(44)	--
P(20)	0.0063(2)	1.550(98)	-0.174(11) 10^{-2}
P(22)	0.0070(3)	1.098(104)	-0.120(20) 10^{-2}
P(24)	0.0085(3)	1.678(110)	-0.108(15) 10^{-2}
P(26)	0.0076(1)	1.516(25)	-0.602(35) 10^{-3}
P(28)	0.0085(5)	1.599(162)	-0.753(236) 10^{-3}
P(30)	0.0093(2)	1.440(47)	-0.809(87) 10^{-3}
P(32)	0.0091(2)	1.686(72)	-0.114(103) 10^{-3}
P(34)	0.0127(1)	1.036(14)	-0.241(5) 10^{-2}
P(36)	0.0106(2)	1.532(42)	-0.158(81) 10^{-3}
P(38)	0.0111(3)	1.389(51)	-0.509(119) 10^{-3}
P(40)	0.0118(2)	1.386(29)	-0.498(72) 10^{-3}
P(42)	0.0136(1)	1.099(3)	-0.176(1) 10^{-2}
P(44)	0.0135(3)	0.853(35)	-0.319(17) 10^{-2}
P(46)	0.0190(4)	0.403(25)	-0.974(28) 10^{-2}

P(48)	0.0138(3)	1.174(51)	-0.132(18) 10^{-2}
P(50)	0.0127(3)	1.885(65)	0.707(110) 10^{-3}
P(52)	0.0179(3)	0.570(25)	-0.689(22) 10^{-2}
P(54)	0.0141(2)	0.624(17)	-0.429(11) 10^{-2}
P(56)	0.0140(5)	2.041(158)	0.115(26) 10^{-2}
P(58)	0.0132(2)	1.954(56)	0.830(93) 10^{-3}
P(60)	-0.0007(1)	-1.504(96)	0.715(45) 10^{-2}
P(62)	0.0135(4)	2.028(102)	0.121(16) 10^{-2}
P(64)	0.0115(2)	2.357(84)	0.164(9) 10^{-2}
P(66)	-0.0191(1)	-0.203(3)	0.269(1) 10^{-1}
P(68)	0.0137(4)	1.201(37)	-0.106(14) 10^{-2}
P(70)	0.0109(5)	0.716(50)	-0.164(26) 10^{-2}
P(72)	0.0207(21)	2.618(168)	0.118(29) 10^{-2}
P(76)	-5.9879(4)	-0.001(1)	0.600(4) 10^{1}
P(78)	-0.0197(2)	-0.347(7)	0.334(3) 10^{-1}
P(80)	0.0249(25)	1.665(138)	--
P(82)	0.0245(4)	1.806(13)	--
P(84)	0.0160(39)	1.430(222)	--
P(86)	0.0084(285)	0.825(296)	--
P(88)	0.0100(7)	0.845(61)	--
P(90)	0.0120(4)	1.500(28)	--

Table 3: The A, B and n parameters obtained from fits of the rCMDS results for the first-order LM coefficients at various temperatures, with the simplified form of the DPL, i.e. $\zeta(T) = A(\frac{T_0}{T})^n + B$. These results are for the sdV profile, those for the Voigt profile being very similar, are not reported here. For some lines, fitting with the DPL was not possible, parameters obtained with the SPL are listed instead. The uncertainties given in parenthesis are multiples of the last significant digit.

Acknowledgments: This work was granted access to the HPC resources of IDRIS under the allocation 2024-*[A0160914906]* made by GENCI. We thank Ryan Cole and Greg Rieker for providing their measured data. Ngoc Hoa Ngo at Hanoi National University of Education (HNUE) gratefully acknowledges the financial support for this research from the National Foundation for Science and Technology Development (NAFOSTED) of Vietnam under grant number 103.03-2023.27.

Reference

[1] S Lebonnois, V Eymet, C Lee, J Vatant d'Ollone. Analysis of the radiative budget of the Venusian atmosphere based on infrared Net Exchange Rate formalism. J Geophys Res Planets 2015;120,1186-200. doi:10.1002/2015JE004794.

[2] CS Goldenstein, RM Spearrin, JB Jeffries, RK Hanson. Infrared laser-absorption sensing for combustion gases. Prog Energy Combust Sci 2017; 60:132-76.

[3] RA Toth, LR Brown, CE Miller, VM Devi, DC Benner. Spectroscopic database of CO_2 line parameters: 4300–7000 cm^{-1}. J Quant Spectrosc Radiat Transf 2008;109:906-921.

[4] A Farooq, JB Jeffries, RK Hanson. CO_2 concentration and temperature sensor for combustion gases using diode-laser absorption near 2.7 μm. Appl Phys B 2008;90:619-28.

[5] L Joly, F Gibert, B Grouiez, A Grossel, B Parvitte, G Durry, V Zeninari. A complete study of CO_2 line parameters around 4845 cm^{-1} for Lidar applications, J Quant Spectrosc Radiat Transf 2008;109:426-34.

[6] JS Li, K Liu, WJ Zhang, WD Chen, XM Gao. Self-, N_2- and O_2-broadening coefficients for the $^{12}C^{16}O_2$ transitions near-IR measured by a diode laser photoacoustic spectrometer. J Mol Spectrosc 2008; 252:9-16.

[7] G Casa, R Wehr, A Castrillo, E Fasci, L Gianfrani, The line shape problem in the near-infrared spectrum of self-colliding CO_2 molecules: Experimental investigation and test of semiclassical models. J Chem Phys 2009;130:184306.

[8] A Predoi-Cross, W Liu, R Murphy, C Povey, RR Gamache, AL Laraia, ARW McKellar, DR Hurtmans, VM Devi. Measurement and computations for temperature dependences of self-broadened carbon dioxide transitions in the 30012←00001 and 30013←00001 bands. J Quant Spectrosc Radiat Transf 2010;111:1065-79.

[9] A Gambetta, D Gatti, A Castrillo, G Galzerano, P Laporta et al. Mid-infrared quantitative spectroscopy by comb-referencing of a quantum-cascade-laser: Application to the CO_2 spectrum at 4.3um, Appl Phys Let 2011;99:251107.

[10] Q Delière, L Fissiaux, M Lepère, Absolute line intensities and self-broadening coefficients in the $\nu_3 - \nu_1$ band of carbon dioxide. J Mol Spectrosc 2012;272:36-42.

[11] NH Ngo, X Landsheere, E Pangui, SB Morales, JM Hartmann. Self-broadening of $^{16}O^{12}C^{16}O$ ν_3-band lines. J Mol Spectrosc 2014;306:33-6.

[12] VM Devi, DC Benner, K Sung, LR Brown, TJ Crawford, CE Miller, BJ Drouin, VH Payne, S Yu, MAH Smith, AW Mantz, RR Gamache. Line parameters including temperature dependences of self- and air-broadened line shapes of $^{12}C^{16}O_2$: 1.6-μm region. J Quant Spectrosc Radiat Transf 2016 ;177:117-44.

[13] H Fleurbaey, H Yi, M Adkins, AJ Fleisher, JT Hodges. Cavity ring-down spectroscopy of CO_2 near $\lambda = 2.06$ μm: Accurate transition intensities for the Orbiting Carbon Observatory-2 (OCO-2) "strong band". J Quant Spectrosc Radiat Transf 2020 ;252:107104.

[14] M Birk, C Röske, G Wagner. High accuracy CO_2 Fourier transform measurements in the range 6000-7000 cm^{-1}. J Quant Spectrosc Radiat Transf 2021;272:107791.

[15] ME Webber, S Kim, ST Sanders, DS Baer, RK Hanson, Y Ikeda. In Situ Combustion Measurements of CO_2 by Use of a Distributed-Feedback Diode-Laser Sensor Near 2.0 μm. Appl Opt 2001;40:821-28.

[16] RK Cole, N Hoghooghi, BJ Drouin, GB Rieker. High-temperature absorption line shape parameters for CO_2 in the 6800–7000 cm^{-1} region from dual frequency comb measurements up to 1000 K. J Quant Spectrosc Radiat Transf 2021;276:107912.

[17] RR Gamache, J Lamouroux. Predicting accurate line shape parameters for CO_2 transitions. J Quant Spectrosc Radiat Transf 2013;130:158-71.

[18] IE Gordon, LS Rothman, RJ Hargreaves, R Hashemi, EV Karlovets, FM Skinner, EK Conway, C Hill, RV Kochanov, Y Tan, P Wcisło, AA Finenko, K Nelson, PF Bernath, M Birk, V Boudon, A Campargue, KV Chance et al.. The HITRAN2020 molecular spectroscopic database. J Quant Spectrosc Radiat Transf 2022;277:107949. https://doi.org/10.1016/j.jqsrt.2021.107949.

[19] R Hashemi, H Rozario, A Ibrahim, A Predoi-Cross. Line shape study of the carbon dioxide laser band. Can J Phys 2013;91:924–36. doi:10.1139/cjp- 2013- 0051.

[20] R Hashemi, IE Gordon, EM Adkins, JT Hodges, DA Long, M Birk, J Loos, CD Boone, AJ Fleisher, A Predoi-Cross, LS Rothman. Intensities, collision-broadened half-widths, and collision-

induced line shifts in the second overtone band of $^{12}C^{16}O$. J Quant Spectrosc Radiat Transf 2021;271:107735.

[21] HT Nguyen, NH Ngo, H Tran. Prediction of line shape parameters and their temperature dependences for CO_2–N_2 using molecular dynamics simulations. J Chem Phys 2018;149:224301. https://doi.org/10.1063/1.5063892

[22] HT Nguyen, NH Ngo, H Tran. Line-shape parameters and their temperature dependences predicted from molecular dynamics simulations for O_2- and air-broadened CO_2 lines. J Quant Spectrosc Radiat Transf 2020;242:106729.

[23] NH Ngo, HT Nguyen, MT Le, H Tran. Air-broadened N_2O line-shape parameters and their temperature dependences by requantized classical molecular dynamics simulations. J Quant Spectrosc Radiat Transf 2021;267:107607.

[24] F Hendaoui, HT Nguyen, H Aroui, NH Ngo, H Tran. Refined line-shape parameters for CO lines broadened by air predicted from requantized classical molecular dynamics simulations. J Quant Spectrosc Radiat Transf 2024;319:108954.

[25] JM Hartmann, H Tran, NH Ngo, X Landsheere, P Chelin, Y Lu, AW Liu, SM Hu, L Gianfrani, G Casa, A Castrillo, M Lepère, Q Delière, M Dhyne, L Fissiaux. *Ab ini t io* calculations of the spectral shapes of CO2 isolated lines including non-Voigt effects and comparisons with experiments. Phys Rev A 2013;87:013403

[26] G Larcher, H Tran, M Schwell, P Chelin, X Landsheere, J-M Hartmann, S-M Hu. CO_2 isolated line shapes by classical molecular dynamics simulations: Influence of the intermolecular potential and comparison with new measurements. J Chem Phys 2014;140:084308.

[27] R Bukowski, J Sadlej, B Jeziorski, P Jankowski, K Szalewicz et al. Intermolecular potential of carbon dioxide dimer from symmetry-adapted perturbation theory. J Chem Phys 1999;110:3785. doi: 10.1063/1.479108.

[28] JM Hartmann, C Boulet, D Jacquemart. Molecular dynamics simulations for CO_2 spectra. II. The far infrared collision-induced absorption band. J Chem Phys 2011;134:094316.

[29] RR Gamache, B Vispoel. On the temperature dependence of half-widths and line shifts for molecular transitions in the microwave and infrared regions. J Quant Spectrosc Radiat Transf 2018;217:440-52.

[30] A Predoi-Cross, W Liu, C Holladay, AV Unni, I Schofield, ARW McKellar, D Hurtmans, Line profile study of transitions in the 30012-00001 and 30013-00001 bands of carbon dioxide perturbed by air. J Mol Spectrosc 2007;246:98-112. doi:10.1016/j.jms.2007.08.008.

[31] JS Wilzewski, M Birk, J Loos, G Wagner. Temperature-Dependence Laws of Absorption Line Shape Parameters of the CO_2 ν_3 Band. J Quant Spectrosc Rad Transfer 2018;206:296-305.

[32] RK Cole, H Tran, N Hoghooghi, GB Rieker. Temperature-dependent CO_2 line mixing models using dual frequency comb absorption and phase spectroscopy up to 25 bar and 1000 K. J Quant Spectrosc Radiat Transf 2023;297:108488